Training Quantized Nets: A Deeper Understanding

Hao Li[1]*, **Soham De**[1]*, **Zheng Xu**[1], **Christoph Studer**[2], **Hanan Samet**[1], **Tom Goldstein**[1]

[1]Department of Computer Science, University of Maryland, College Park
[2]School of Electrical and Computer Engineering, Cornell University
{haoli,sohamde,xuzh,hjs,tomg}@cs.umd.edu, studer@cornell.edu

Abstract

Currently, deep neural networks are deployed on low-power portable devices by first training a full-precision model using powerful hardware, and then deriving a corresponding low-precision model for efficient inference on such systems. However, training models directly with coarsely quantized weights is a key step towards learning on embedded platforms that have limited computing resources, memory capacity, and power consumption. Numerous recent publications have studied methods for training quantized networks, but these studies have mostly been empirical. In this work, we investigate training methods for quantized neural networks from a theoretical viewpoint. We first explore accuracy guarantees for training methods under convexity assumptions. We then look at the behavior of these algorithms for non-convex problems, and show that training algorithms that exploit high-precision representations have an important greedy search phase that purely quantized training methods lack, which explains the difficulty of training using low-precision arithmetic.

1   Introduction

Deep neural networks are an integral part of state-of-the-art computer vision and natural language processing systems. Because of their high memory requirements and computational complexity, networks are usually trained using powerful hardware. There is an increasing interest in training and deploying neural networks directly on battery-powered devices, such as cell phones or other platforms. Such low-power embedded systems are memory and power limited, and in some cases lack basic support for floating-point arithmetic.

To make neural nets practical on embedded systems, many researchers have focused on training nets with *coarsely quantized* weights. For example, weights may be constrained to take on integer/binary values, or may be represented using low-precision (8 bits or less) fixed-point numbers. Quantized nets offer the potential of superior memory and computation efficiency, while achieving performance that is competitive with state-of-the-art high-precision nets. Quantized weights can dramatically reduce memory size and access bandwidth, increase power efficiency, exploit hardware-friendly bitwise operations, and accelerate inference throughput [1–3].

Handling low-precision weights is difficult and motivates interest in new training methods. When learning rates are small, stochastic gradient methods make small updates to weight parameters. Binarization/discretization of weights after each training iteration "rounds off" these small updates and causes training to stagnate [1]. Thus, the naïve approach of quantizing weights using a rounding procedure yields poor results when weights are represented using a small number of bits. Other approaches include classical stochastic rounding methods [4], as well as schemes that combine full-precision floating-point weights with discrete rounding procedures [5]. While some of these schemes seem to work in practice, results in this area are largely experimental, and little work has been devoted to explaining the excellent performance of some methods, the poor performance of others, and the important differences in behavior between these methods.

---

*Equal contribution. Author ordering determined by a cryptographically secure random number generator.

Contributions This paper studies quantized training methods from a theoretical perspective, with the goal of understanding the differences in behavior, and reasons for success or failure, of various methods. In particular, we present a convergence analysis showing that classical stochastic rounding (SR) methods [4] as well as newer and more powerful methods like BinaryConnect (BC) [5] are capable of solving convex discrete problems up to a level of accuracy that depends on the quantization level. We then address the issue of why algorithms that maintain floating-point representations, like BC, work so well, while fully quantized training methods like SR stall before training is complete. We show that the long-term behavior of BC has an important annealing property that is needed for non-convex optimization, while classical rounding methods lack this property.

2   Background and Related Work

The arithmetic operations of deep networks can be truncated down to 8-bit fixed-point without significant deterioration in inference performance [4, 6–9]. The most extreme scenario of quantization is binarization, in which only 1-bit (two states) is used for weight representation [10, 5, 1, 3, 11, 12].

Previous work on obtaining a quantized neural network can be divided into two categories: quantizing pre-trained models with or without retraining [7, 13, 6, 14, 15], and training a quantized model from scratch [4, 5, 3, 1, 16]. We focus on approaches that belong to the second category, as they can be used for both training and inference under constrained resources.

For training quantized NNs from scratch, many authors suggest maintaining a high-precision floating point copy of the weights while feeding quantized weights into backprop [5, 11, 3, 16], which results in good empirical performance. There are limitations in using such methods on low-power devices, however, where floating-point arithmetic is not always available or not desirable. Another widely used solution using only low-precision weights is *stochastic rounding* [17, 4]. Experiments show that networks using 16-bit fixed-point representations with stochastic rounding can deliver results nearly identical to 32-bit floating-point computations [4], while lowering the precision down to 3-bit fixed-point often results in a significant performance degradation [18]. Bayesian learning has also been applied to train binary networks [19, 20]. A more comprehensive review can be found in [3].

3   Training Quantized Neural Nets

We consider empirical risk minimization problems of the form:

$$\min_{w \in \mathcal{W}} F(w) := \frac{1}{m} \sum_{i=1}^{m} f_i(w), \tag{1}$$

where the objective function decomposes into a sum over many functions $f_i : \mathbb{R}^d \to \mathbb{R}$. Neural networks have objective functions of this form where each f_i is a non-convex loss function. When floating-point representations are available, the standard method for training neural networks is stochastic gradient descent (SGD), which on each iteration selects a function $\tilde{f}$ randomly from $\{f_1, f_2, \ldots, f_m\}$, and then computes

$$\text{SGD: } w^{t+1} = w^t - \alpha_t \nabla \tilde{f}(w^t), \tag{2}$$

for some learning rate α_t. In this paper, we consider the problem of training convolutional neural networks (CNNs). Convolutions are computationally expensive; low precision weights can be used to accelerate them by replacing expensive multiplications with efficient addition and subtraction operations [3, 9] or bitwise operations [11, 16].

To train networks using a low-precision representation of the weights, a quantization function $Q(\cdot)$ is needed to convert a real-valued number w into a quantized/rounded version $\hat{w} = Q(w)$. We use the same notation for quantizing vectors, where we assume Q acts on each dimension of the vector. Different quantized optimization routines can be defined by selecting different quantizers, and also by selecting when quantization happens during optimization. The common options are:

Deterministic Rounding (R) A basic *uniform* or deterministic quantization function snaps a floating point value to the closest quantized value as:

$$Q_d(w) = \text{sign}(w) \cdot \Delta \cdot \left\lfloor \frac{|w|}{\Delta} + \frac{1}{2} \right\rfloor, \tag{3}$$

2

where Δ denotes the quantization step or resolution, i.e., the smallest positive number that is representable. One exception to this definition is when we consider binary weights, where all weights are constrained to have two values $w \in \{-1, 1\}$ and uniform rounding becomes $Q_d(w) = \text{sign}(w)$.

The deterministic rounding SGD maintains quantized weights with updates of the form:

$$\text{Deterministic Rounding: } w_b^{t+1} = Q_d\big(w_b^t - \alpha_t \nabla \tilde{f}(w_b^t)\big), \tag{4}$$

where w_b denotes the low-precision weights, which are quantized using Q_d immediately after applying the gradient descent update. If gradient updates are significantly smaller than the quantization step, this method loses gradient information and weights may never be modified from their starting values.

Stochastic Rounding (SR) The quantization function for *stochastic rounding* is defined as:

$$Q_s(w) = \Delta \cdot \begin{cases} \lfloor \frac{w}{\Delta} \rfloor + 1 & \text{for } p \leq \frac{w}{\Delta} - \lfloor \frac{w}{\Delta} \rfloor, \\ \lfloor \frac{w}{\Delta} \rfloor & \text{otherwise,} \end{cases} \tag{5}$$

where $p \in [0, 1]$ is produced by a uniform random number generator. This operator is non-deterministic, and rounds its argument up with probability $w/\Delta - \lfloor w/\Delta \rfloor$, and down otherwise. This quantizer satisfies the important property $\mathbb{E}[Q_s(w)] = w$. Similar to the deterministic rounding method, the SR optimization method also maintains quantized weights with updates of the form:

$$\text{Stochastic Rounding: } w_b^{t+1} = Q_s\big(w_b^t - \alpha_t \nabla \tilde{f}(w_b^t)\big). \tag{6}$$

BinaryConnect (BC) The BinaryConnect algorithm [5] accumulates gradient updates using a full-precision buffer w_r, and quantizes weights just before gradient computations as follows.

$$\text{BinaryConnect: } w_r^{t+1} = w_r^t - \alpha_t \nabla \tilde{f}\big(Q(w_r^t)\big). \tag{7}$$

Either stochastic rounding Q_s or deterministic rounding Q_d can be used for quantizing the weights w_r, but in practice, Q_d is the common choice. The original BinaryConnect paper constrains the low-precision weights to be $\{-1, 1\}$, which can be generalized to $\{-\Delta, \Delta\}$. A more recent method, Binary-Weights-Net (BWN) [3], allows different filters to have different scales for quantization, which often results in better performance on large datasets.

Notation For the rest of the paper, we use Q to denote both Q_s and Q_d unless the situation requires this to be distinguished. We also drop the subscripts on w_r and w_b, and simply write w.

4 Convergence Analysis

We now present convergence guarantees for the Stochastic Rounding (SR) and BinaryConnect (BC) algorithms, with updates of the form (6) and (7), respectively. For the purposes of deriving theoretical guarantees, we assume each f_i in (1) is differentiable and convex, and the domain $\mathcal{W}$ is convex and has dimension d. We consider both the case where F is μ-strongly convex: $\langle \nabla F(w'), w - w' \rangle \leq F(w) - F(w') - \frac{\mu}{2}\|w - w'\|^2$, as well as where F is weakly convex. We also assume the (stochastic) gradients are bounded: $\mathbb{E}\|\nabla \tilde{f}(w^t)\|^2 \leq G^2$. Some results below also assume the domain of the problem is finite. In this case, the rounding algorithm clips values that leave the domain. For example, in the binary case, rounding returns bounded values in $\{-1, 1\}$.

4.1 Convergence of Stochastic Rounding (SR)

We can rewrite the update rule (6) as:

$$w^{t+1} = w^t - \alpha_t \nabla \tilde{f}(w^t) + r^t,$$

where $r^t = Q_s(w^t - \alpha_t \nabla \tilde{f}(w^t)) - w^t + \alpha_t \nabla \tilde{f}(w^t)$ denotes the quantization error on the t-th iteration. We want to bound this error in expectation. To this end, we present the following lemma.

Lemma 1. *The stochastic rounding error r^t on each iteration can be bounded, in expectation, as:*

$$\mathbb{E}\|r^t\|^2 \leq \sqrt{d}\Delta\alpha_t G,$$

where d denotes the dimension of w.

3

Proofs for all theoretical results are presented in the Appendices. From Lemma 1, we see that the rounding error per step decreases as the learning rate α_t decreases. This is intuitive since the probability of an entry in w^{t+1} differing from w^t is small when the gradient update is small relative to Δ. Using the above lemma, we now present convergence rate results for Stochastic Rounding (SR) in both the strongly-convex case and the non-strongly convex case. Our error estimates are ergodic, i.e., they are in terms of $\bar{w}^T = \frac{1}{T}\sum_{t=1}^{T} w^t$, the average of the iterates.

Theorem 1. *Assume that F is μ-strongly convex and the learning rates are given by $\alpha_t = \frac{1}{\mu(t+1)}$. Consider the SR algorithm with updates of the form* (6). *Then, we have:*

$$\mathbb{E}[F(\bar{w}^T) - F(w^\star)] \leq \frac{(1 + \log(T+1))G^2}{2\mu T} + \frac{\sqrt{d}\Delta G}{2},$$

where $w^\star = \arg\min_w F(w)$.

Theorem 2. *Assume the domain has finite diameter D, and learning rates are given by $\alpha_t = \frac{c}{\sqrt{t}}$, for a constant c. Consider the SR algorithm with updates of the form* (6). *Then, we have:*

$$\mathbb{E}[F(\bar{w}^T) - F(w^\star)] \leq \frac{1}{c\sqrt{T}}D^2 + \frac{\sqrt{T+1}}{2T}cG^2 + \frac{\sqrt{d}\Delta G}{2}.$$

We see that in both cases, SR converges until it reaches an "accuracy floor." As the quantization becomes more fine grained, our theory predicts that the accuracy of SR approaches that of high-precision floating point at a rate linear in Δ. This extra term caused by the discretization is unavoidable since this method maintains quantized weights.

4.2 Convergence of Binary Connect (BC)

When analyzing the BC algorithm, we assume that the Hessian satisfies the Lipschitz bound: $\|\nabla^2 f_i(x) - \nabla^2 f_i(y)\| \leq L_2\|x - y\|$ for some $L_2 \geq 0$. While this is a slightly non-standard assumption, we will see that it enables us to gain better insights into the behavior of the algorithm.

The results here hold for both stochastic and uniform rounding. In this case, the quantization error r does not approach 0 as in SR-SGD. Nonetheless, the effect of this rounding error diminishes with shrinking α_t because α_t multiplies the gradient update, and thus implicitly the rounding error as well.

Theorem 3. *Assume F is L-Lipschitz smooth, the domain has finite diameter D, and learning rates are given by $\alpha_t = \frac{c}{\sqrt{t}}$. Consider the BC-SGD algorithm with updates of the form* (7). *Then, we have:*

$$\mathbb{E}[F(\bar{w}^T) - F(w^\star)] \leq \frac{1}{2c\sqrt{T}}D^2 + \frac{\sqrt{T+1}}{2T}cG^2 + \sqrt{d}\Delta LD.$$

As with SR, BC can only converge up to an error floor. So far this looks a lot like the convergence guarantees for SR. However, things change when we assume strong convexity and bounded Hessian.

Theorem 4. *Assume that F is μ-strongly convex and the learning rates are given by $\alpha_t = \frac{1}{\mu(t+1)}$. Consider the BC algorithm with updates of the form* (7). *Then we have:*

$$\mathbb{E}[F(\bar{w}^T) - F(w^\star)] \leq \frac{(1 + \log(T+1))G^2}{2\mu T} + \frac{DL_2\sqrt{d}\Delta}{2}.$$

Now, the error floor is determined by both Δ and L_2. For a quadratic least-squares problem, the gradient of F is linear and the Hessian is constant. Thus, $L_2 = 0$ and we get the following corollary.

Corollary 1. *Assume that F is quadratic and the learning rates are given by $\alpha_t = \frac{1}{\mu(t+1)}$. The BC algorithm with updates of the form* (7) *yields*

$$\mathbb{E}[F(\bar{w}^T) - F(w^\star)] \leq \frac{(1 + \log(T+1))G^2}{2\mu T}.$$

We see that the real-valued weights accumulated in BC can converge to the *true minimizer* of quadratic losses. Furthermore, this suggests that, when the function behaves like a quadratic on the distance
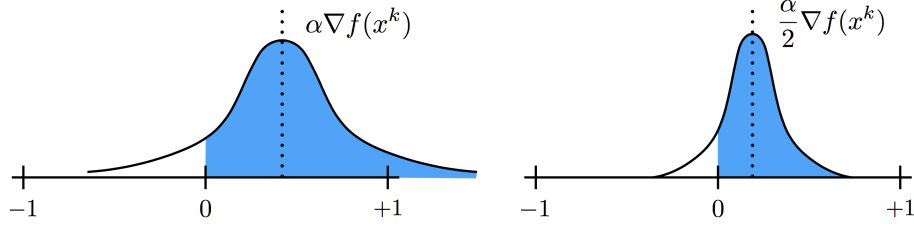
Figure 1: The SR method starts at some location x (in this case 0), adds a perturbation to x, and then rounds. As the learning rate α gets smaller, the distribution of the perturbation gets "squished" near the origin, making the algorithm less likely to move. The "squishing" effect is the same for the part of the distribution lying to the left and to the right of x, and so it does not effect the *relative* probability of moving left or right.

scale Δ, one would expect BC to perform fundamentally better than SR. While this may seem like a restrictive condition, there is evidence that even non-convex neural networks become well approximated as a quadratic in the later stages of optimization within a neighborhood of a local minimum [21].

Note, our convergence results on BC are for w_r instead of w_b, and these measures of convergence are not directly comparable. It is not possible to bound w_b when BC is used, as the values of w_b may not converge in the usual sense (e.g., in the +/-1 binary case w_r might converge to 0, in which case arbitrarily small perturbations to w_r might send w_b to +1 or -1).

5 What About Non-Convex Problems?

The global convergence results presented above for convex problems show that, in general, both the SR and BC algorithms converge to within $\mathcal{O}(\Delta)$ accuracy of the minimizer (in expected value). However, these results do not explain the large differences between these methods when applied to non-convex neural nets. We now study how the long-term behavior of SR differs from BC. Note that this section makes no convexity assumptions, and the proposed theoretical results are directly applicable to neural networks.

Typical (continuous-valued) SGD methods have an important exploration-exploitation tradeoff. When the learning rate is large, the algorithm explores by moving quickly between states. Exploitation happens when the learning rate is small. In this case, noise averaging causes the algorithm more greedily pursues local minimizers with lower loss values. Thus, the distribution of iterates produced by the algorithm becomes increasingly concentrated near minimizers as the learning rate vanishes (see, e.g., the large-deviation estimates in [22]). BC maintains this property as well—indeed, we saw in Corollary 1 a class of problems for which the iterates concentrate on the minimizer for small α_t.

In this section, we show that the SR method lacks this important tradeoff: as the stepsize gets small and the algorithm slows down, the quality of the iterates produced by the algorithm does *not* improve, and the algorithm does *not* become progressively more likely to produce low-loss iterates. This behavior is illustrated in Figures 1 and 2.

To understand this problem conceptually, consider the simple case of a one-variable optimization problem starting at $x^0 = 0$ with $\Delta = 1$ (Figure 1). On each iteration, the algorithm computes a stochastic approximation $\nabla \tilde{f}$ of the gradient by sampling from a distribution, which we call p. This gradient is then multiplied by the stepsize to get $\alpha \nabla \tilde{f}$. The probability of moving to the right (or left) is then roughly proportional to the magnitude of $\alpha \nabla \tilde{f}$. Note the random variable $\alpha \nabla \tilde{f}$ has distribution $p_\alpha(z) = \alpha^{-1} p(z/\alpha)$.

Now, suppose that α is small enough that we can neglect the tails of $p_\alpha(z)$ that lie outside the interval $[-1, 1]$. The probability of transitioning from $x^0 = 0$ to $x^1 = 1$ using stochastic rounding, denoted by $T_\alpha(0, 1)$, is then

$$T_\alpha(0,1) \approx \int_0^1 z p_\alpha(z) dz = \frac{1}{\alpha} \int_0^1 z p(z/\alpha)\, dz = \alpha \int_0^{1/\alpha} p(x) x\, dx \approx \alpha \int_0^\infty p(x) x\, dx,$$

where the first approximation is because we neglected the unlikely case that $\alpha \nabla \tilde{f} > 1$, and the second approximation appears because we added a small tail probability to the estimate. These
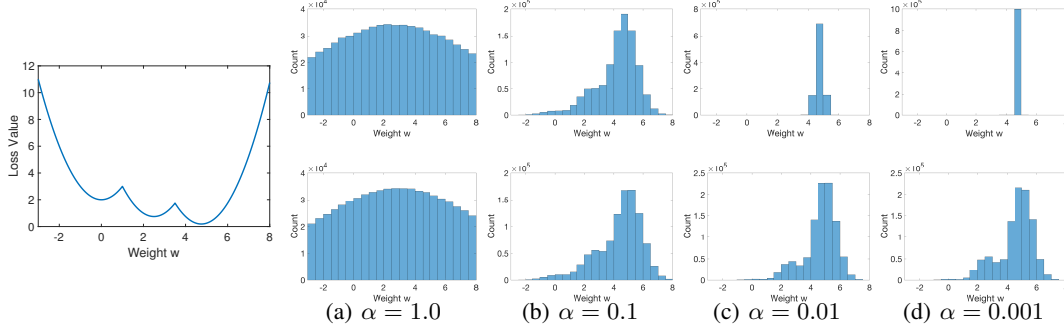
Figure 2: Effect of shrinking the learning rate in SR vs BC on a toy problem. The left figure plots the objective function (8). Histograms plot the distribution of the quantized weights over 10^6 iterations. The top row of plots correspond to BC, while the bottom row is SR, for different learning rates α. As the learning rate α shrinks, the BC distribution concentrates on a minimizer, while the SR distribution stagnates.

approximations get more accurate for small α. We see that, assuming the tails of p are "light" enough, we have $T_\alpha(0,1) \sim \alpha \int_0^\infty p(x)x\,dx$ as $\alpha \to 0$. Similarly, $T_\alpha(0,-1) \sim \alpha \int_{-\infty}^0 p(x)x\,dx$ as $\alpha \to 0$.

What does this observation mean for the behavior of SR? First of all, the probability of leaving x^0 on an iteration is

$$T_\alpha(0,-1) + T_\alpha(0,1) \approx \alpha \left[\int_0^\infty p(x)x\,dx + \int_{-\infty}^0 p(x)x\,dx \right],$$

which vanishes for small α. This means the algorithm slows down as the learning rate drops off, which is not surprising. However, the *conditional* probability of ending up at $x^1 = 1$ given that the algorithm *did* leave x^0 is

$$T_\alpha(0,1|x^1 \neq x^0) \approx \frac{T_\alpha(0,1)}{T_\alpha(0,-1) + T_\alpha(0,1)} = \frac{\int_0^\infty p(x)x\,dx}{\int_{-\infty}^0 p(x)x\,dx + \int_0^\infty p(x)x\,dx},$$

which does not depend on α. In other words, provided α is small, SR, on average, makes the same decisions/transitions with learning rate α as it does with learning rate $\alpha/10$; it just takes 10 times longer to make those decisions when $\alpha/10$ is used. In this situation, there is no exploitation benefit in decreasing α.

5.1 Toy Problem

To gain more intuition about the effect of shrinking the learning rate in SR vs BC, consider the following simple 1-dimensional non-convex problem:

$$\min_w f(w) := \begin{cases} w^2 + 2, & \text{if } w < 1, \\ (w - 2.5)^2 + 0.75, & \text{if } 1 \leq w < 3.5, \\ (w - 4.75)^2 + 0.19, & \text{if } w \geq 3.5. \end{cases} \tag{8}$$

Figure 2 shows a plot of this loss function. To visualize the distribution of iterates, we initialize at $w = 4.0$, and run SR and BC for 10^6 iterations using a quantization resolution of 0.5.

Figure 2 shows the distribution of the quantized weight parameters w over the iterations when optimized with SR and BC for different learning rates α. As we shift from $\alpha = 1$ to $\alpha = 0.001$, the distribution of BC iterates transitions from a wide/explorative distribution to a narrow distribution in which iterates aggressively concentrate on the minimizer. In contrast, the distribution produced by SR concentrates only slightly and then stagnates; the iterates are spread widely even when the learning rate is small.

5.2 Asymptotic Analysis of Stochastic Rounding

The above argument is intuitive, but also informal. To make these statements rigorous, we interpret the SR method as a Markov chain. On each iteration, SR starts at some state (iterate) x, and moves to
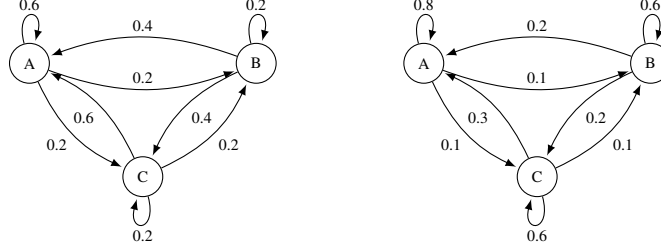
Figure 3: Markov chain example with 3 states. In the right figure, we halved each transition probability for moving between states, with the remaining probability put on the self-loop. Notice that halving all the transition probabilities would not change the equilibrium distribution, and instead would only increase the mixing time of the Markov chain.

a new state y with some transition probability $T_\alpha(x, y)$ that depends only on x and the learning rate α. For fixed α, this is clearly a Markov process with transition matrix[2] $T_\alpha(x, y)$.

The long-term behavior of this Markov process is determined by the *stationary distribution* of $T_\alpha(x, y)$. We show below that for small α, the stationary distribution of $T_\alpha(x, y)$ is nearly invariant to α, and thus decreasing α below some threshold has virtually no effect on the long term behavior of the method. This happens because, as α shrinks, the relative transition probabilities remain the same (conditioned on the fact that the parameters change), even though the absolute probabilities decrease (see Figure 3). In this case, there is no exploitation benefit to decreasing α.

Theorem 5. *Let $p_{x,k}$ denote the probability distribution of the kth entry in $\nabla \tilde{f}(x)$, the stochastic gradient estimate at x. Assume there is a constant C_1 such that for all x, k, and ν we have $\int_\nu^\infty p_{x,k}(z)\,dz \le \frac{C_1}{\nu^2}$, and some C_2 such that both $\int_0^{C_2} p_{x,k}(z)\,dz > 0$ and $\int_{-C_2}^0 p_{x,k}(z)\,dz > 0$. Define the matrix*

$$\tilde{U}(x, y) = \begin{cases} \int_0^\infty p_{x,k}(z)\frac{z}{\Delta}\,dz, & \textit{if } x \textit{ and } y \textit{ differ only at coordinate } k, \textit{ and } y_k = x_k + \Delta \\ \int_{-\infty}^0 p_{x,k}(z)\frac{z}{\Delta}\,dz, & \textit{if } x \textit{ and } y \textit{ differ only at coordinate } k, \textit{ and } y_k = x_k - \Delta \\ 0, & \textit{otherwise,} \end{cases}$$

and the associated markov chain transition matrix

$$\tilde{T}_{\alpha_0} = I - \alpha_0 \cdot \mathrm{diag}(\mathbf{1}^T \tilde{U}) + \alpha_0 \tilde{U}, \tag{9}$$

where α_0 is the largest constant that makes $\tilde{T}_{\alpha_0}$ non-negative. Suppose $\tilde{T}_\alpha$ has a stationary distribution, denoted $\tilde{\pi}$. Then, for sufficiently small α, T_α has a stationary distribution π_α, and

$$\lim_{\alpha \to 0} \pi_\alpha = \tilde{\pi}.$$

Furthermore, this limiting distribution satisfies $\tilde{\pi}(x) > 0$ for any state x, and is thus not concentrated on local minimizers of f.

While the long term stationary behavior of SR is relatively insensitive to α, the convergence speed of the algorithm is not. To measure this, we consider the *mixing time* of the Markov chain. Let π_α denote the stationary distribution of a Markov chain. We say that the ϵ-mixing time of the chain is M_ϵ if M_ϵ is the smallest integer such that [23]

$$|\mathbb{P}(x^{M_\epsilon} \in A | x^0) - \pi(A)| \le \epsilon, \quad \text{for all } x^0 \text{ and all subsets of states } A \subseteq X. \tag{10}$$

We show below that the mixing time of the Markov chain gets large for small α, which means exploration slows down, even though no exploitation gain is being realized.

Theorem 6. *Let $p_{x,k}$ satisfy the assumptions of Theorem 5. Choose some ϵ sufficiently small that there exists a* proper *subset of states $A \subset X$ with stationary probability $\pi_\alpha(A)$ greater than ϵ. Let $M_\epsilon(\alpha)$ denote the ϵ-mixing time of the chain with learning rate α. Then,*

$$\lim_{\alpha \to 0} M_\epsilon(\alpha) = \infty.$$

---

[2]Our analysis below does not require the state space to be finite, so $T_\alpha(x, y)$ may be a linear operator rather than a matrix. Nonetheless, we use the term "matrix" as it is standard.

Table 1: Top-1 test error after training with full-precision (ADAM), binarized weights (R-ADAM, SR-ADAM, BC-ADAM), and binarized weights with big batch size (Big SR-ADAM).

	CIFAR-10				CIFAR-100	ImageNet
	VGG-9	VGG-BC	ResNet-56	WRN-56-2	ResNet-56	ResNet-18
ADAM	7.97	7.12	8.10	6.62	33.98	36.04
BC-ADAM	10.36	8.21	8.83	7.17	35.34	52.11
Big SR-ADAM	16.95	16.77	19.84	16.04	50.79	77.68
SR-ADAM	23.33	20.56	26.49	21.58	58.06	88.86
R-ADAM	23.99	21.88	33.56	27.90	68.39	91.07

6 Experiments

To explore the implications of the theory above, we train both VGG-like networks [24] and Residual networks [25] with binarized weights on image classification problems. On CIFAR-10, we train ResNet-56, wide ResNet-56 (WRN-56-2, with 2X more filters than ResNet-56), VGG-9, and the high capacity VGG-BC network used for the original BC model [5]. We also train ResNet-56 on CIFAR-100, and ResNet-18 on ImageNet [26].

We use Adam [27] as our baseline optimizer as we found it to frequently give better results than well-tuned SGD (an observation that is consistent with previous papers on quantized models [1–5]), and we train with the three quantized algorithms mentioned in Section 3, i.e., R-ADAM, SR-ADAM and BC-ADAM. The image pre-processing and data augmentation procedures are the same as [25]. Following [3], we only quantize the weights in the convolutional layers, but not linear layers, during training (See Appendix H.1 for a discussion of this issue, and a detailed description of experiments).

We set the initial learning rate to 0.01 and decrease the learning rate by a factor of 10 at epochs 82 and 122 for CIFAR-10 and CIFAR-100 [25]. For ImageNet experiments, we train the model for 90 epochs and decrease the learning rate at epochs 30 and 60. See Appendix H for additional experiments.

Results The overall results are summarized in Table 1. The binary model trained by BC-ADAM has comparable performance to the full-precision model trained by ADAM. SR-ADAM outperforms R-ADAM, which verifies the effectiveness of Stochastic Rounding. There is a performance gap between SR-ADAM and BC-ADAM across all models and datasets. This is consistent with our theoretical results in Sections 4 and 5, which predict that keeping track of the real-valued weights as in BC-ADAM should produce better minimizers.

Exploration vs exploitation tradeoffs Section 5 discusses the exploration/exploitation tradeoff of continuous-valued SGD methods and predicts that fully discrete methods like SR are unable to enter a greedy phase. To test this effect, we plot the percentage of changed weights (signs different from the initialization) as a function of the training epochs (Figures 4 and 5). SR-ADAM explores aggressively; it changes more weights in the conv layers than both R-ADAM and BC-ADAM, and keeps changing weights until nearly 40% of the weights differ from their starting values (in a binary model, randomly re-assigning weights would result in 50% change). The BC method never changes more than 20% of the weights (Fig 4(b)), indicating that it stays near a local minimizer and explores less. Interestingly, we see that the weights of the conv layers were not changed at all by R-ADAM; when the tails of the stochastic gradient distribution are light, this method is ineffective.

6.1 A Way Forward: Big Batch Training

We saw in Section 5 that SR is unable to exploit local minima because, for small learning rates, shrinking the learning rate does not produce additional bias towards moving downhill. This was illustrated in Figure 1. If this is truly the cause of the problem, then our theory predicts that we can improve the performance of SR for low-precision training by increasing the batch size. This shrinks the variance of the gradient distribution in Figure 1 without changing the mean and concentrates more of the gradient distribution towards downhill directions, making the algorithm more greedy.

To verify this, we tried different batch sizes for SR including 128, 256, 512 and 1024, and found that the larger the batch size, the better the performance of SR. Figure 5(a) illustrates the effect of a batch size of 1024 for BC and SR methods. We find that the BC method, like classical SGD, performs best
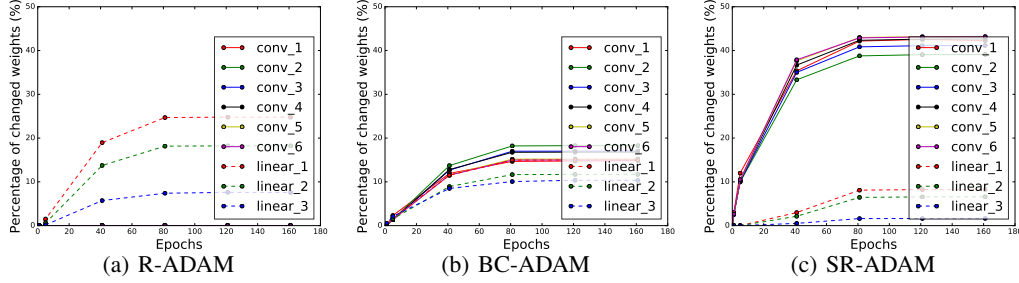
(a) R-ADAM   (b) BC-ADAM   (c) SR-ADAM

Figure 4: Percentage of weight changes during training of VGG-BC on CIFAR-10.

(a) BC-ADAM vs SR-ADAM   (b) Weight changes since beginning   (c) Weight changes every 5 epochs
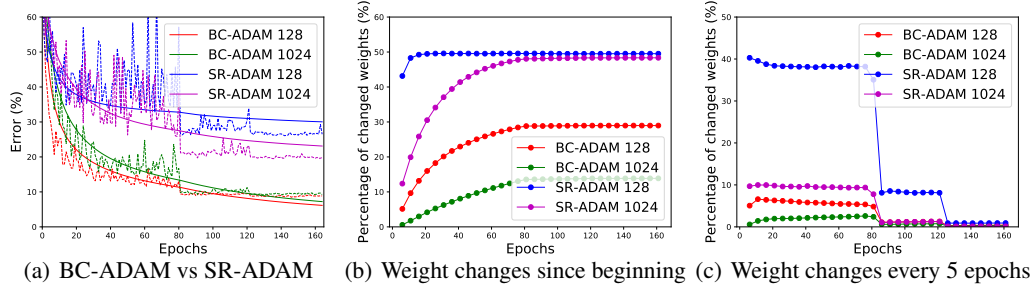
Figure 5: Effect of batch size on SR-ADAM when tested with ResNet-56 on CIFAR-10. (a) Test error vs epoch. Test error is reported with dashed lines, train error with solid lines. (b) Percentage of weight changes since initialization. (c) Percentage of weight changes per every 5 epochs.

with a small batch size. However, a large batch size is essential for the SR method to perform well. Figure 5(b) shows the percentage of weights changed by SR and BC during training. We see that the large batch methods change the weights less aggressively than the small batch methods, indicating less exploration. Figure 5(c) shows the percentage of weights changed during each 5 epochs of training. It is clear that small-batch SR changes weights much more frequently than using a big batch. This property of big batch training clearly benefits SR; we see in Figure 5(a) and Table 1 that big batch training improved performance over SR-ADAM consistently.

In addition to providing a means of improving fixed-point training, this suggests that recently proposed methods using big batches [28, 29] may be able to exploit lower levels of precision to further accelerate training.

7   Conclusion

The training of quantized neural networks is essential for deploying machine learning models on portable and ubiquitous devices. We provide a theoretical analysis to better understand the BinaryConnect (BC) and Stochastic Rounding (SR) methods for training quantized networks. We proved convergence results for BC and SR methods that predict an accuracy bound that depends on the coarseness of discretization. For general non-convex problems, we proved that SR differs from conventional stochastic methods in that it is unable to exploit greedy local search. Experiments confirm these findings, and show that the mathematical properties of SR are indeed observable (and very important) in practice.

Acknowledgments

9

References

[1] Courbariaux, M., Hubara, I., Soudry, D., El-Yaniv, R., Bengio, Y.: Binarized neural networks: Training deep neural networks with weights and activations constrained to +1 or -1. arXiv preprint arXiv:1602.02830 (2016)

[2] Marchesi, M., Orlandi, G., Piazza, F., Uncini, A.: Fast neural networks without multipliers. IEEE Transactions on Neural Networks **4**(1) (1993) 53–62

[3] Rastegari, M., Ordonez, V., Redmon, J., Farhadi, A.: XNOR-Net: ImageNet Classification Using Binary Convolutional Neural Networks. ECCV (2016)

[4] Gupta, S., Agrawal, A., Gopalakrishnan, K., Narayanan, P.: Deep learning with limited numerical precision. In: ICML. (2015)

[5] Courbariaux, M., Bengio, Y., David, J.P.: Binaryconnect: Training deep neural networks with binary weights during propagations. In: NIPS. (2015)

[6] Lin, D., Talathi, S., Annapureddy, S.: Fixed point quantization of deep convolutional networks. In: ICML. (2016)

[7] Hwang, K., Sung, W.: Fixed-point feedforward deep neural network design using weights+ 1, 0, and- 1. In: IEEE Workshop on Signal Processing Systems (SiPS). (2014)

[8] Lin, Z., Courbariaux, M., Memisevic, R., Bengio, Y.: Neural networks with few multiplications. ICLR (2016)

[9] Li, F., Zhang, B., Liu, B.: Ternary weight networks. arXiv preprint arXiv:1605.04711 (2016)

[10] Kim, M., Smaragdis, P.: Bitwise neural networks. In: ICML Workshop on Resource-Efficient Machine Learning. (2015)

[11] Hubara, I., Courbariaux, M., Soudry, D., El-Yaniv, R., Bengio, Y.: Quantized neural networks: Training neural networks with low precision weights and activations. arXiv preprint arXiv:1609.07061 (2016)

[12] Baldassi, C., Ingrosso, A., Lucibello, C., Saglietti, L., Zecchina, R.: Subdominant dense clusters allow for simple learning and high computational performance in neural networks with discrete synapses. Physical review letters **115**(12) (2015) 128101

[13] Anwar, S., Hwang, K., Sung, W.: Fixed point optimization of deep convolutional neural networks for object recognition. In: ICASSP, IEEE (2015)

[14] Zhu, C., Han, S., Mao, H., Dally, W.J.: Trained ternary quantization. ICLR (2017)

[15] Zhou, A., Yao, A., Guo, Y., Xu, L., Chen, Y.: Incremental network quantization: Towards lossless CNNs with low-precision weights. ICLR (2017)

[16] Zhou, S., Wu, Y., Ni, Z., Zhou, X., Wen, H., Zou, Y.: Dorefa-net: Training low bitwidth convolutional neural networks with low bitwidth gradients. arXiv preprint arXiv:1606.06160 (2016)

[17] Höhfeld, M., Fahlman, S.E.: Probabilistic rounding in neural network learning with limited precision. Neurocomputing **4**(6) (1992) 291–299

[18] Miyashita, D., Lee, E.H., Murmann, B.: Convolutional neural networks using logarithmic data representation. arXiv preprint arXiv:1603.01025 (2016)

[19] Soudry, D., Hubara, I., Meir, R.: Expectation backpropagation: Parameter-free training of multilayer neural networks with continuous or discrete weights. In: NIPS. (2014)

[20] Cheng, Z., Soudry, D., Mao, Z., Lan, Z.: Training binary multilayer neural networks for image classification using expectation backpropagation. arXiv preprint arXiv:1503.03562 (2015)

[21] Martens, J., Grosse, R.: Optimizing neural networks with kronecker-factored approximate curvature. In: International Conference on Machine Learning. (2015) 2408–2417

[22] Lan, G., Nemirovski, A., Shapiro, A.: Validation analysis of mirror descent stochastic approximation method. Mathematical programming **134**(2) (2012) 425–458

[23] Levin, D.A., Peres, Y., Wilmer, E.L.: Markov chains and mixing times. American Mathematical Soc. (2009)

[24] Simonyan, K., Zisserman, A.: Very Deep Convolutional Networks for Large-Scale Image Recognition. In: ICLR. (2015)

[25] He, K., Zhang, X., Ren, S., Sun, J.: Deep Residual Learning for Image Recognition. In: CVPR. (2016)

[26] Russakovsky, O., Deng, J., Su, H., Krause, J., Satheesh, S., Ma, S., Huang, Z., Karpathy, A., Khosla, A., Bernstein, M., et al.: Imagenet Large Scale Visual Recognition Challenge. IJCV (2015)

[27] Kingma, D., Ba, J.: Adam: A method for stochastic optimization. ICLR (2015)

[28] De, S., Yadav, A., Jacobs, D., Goldstein, T.: Big batch SGD: Automated inference using adaptive batch sizes. arXiv preprint arXiv:1610.05792 (2016)

[29] Goyal, P., Dollár, P., Girshick, R., Noordhuis, P., Wesolowski, L., Kyrola, A., Tulloch, A., Jia, Y., He, K.: Accurate, large minibatch sgd: Training imagenet in 1 hour. arXiv preprint arXiv:1706.02677 (2017)

[30] Lax, P.: Linear Algebra and Its Applications. Number v. 10 in Linear algebra and its applications. Wiley (2007)

[31] Krizhevsky, A.: Learning multiple layers of features from tiny images. (2009)

[32] Zagoruyko, S., Komodakis, N.: Wide residual networks. arXiv preprint arXiv:1605.07146 (2016)

[33] Collobert, R., Kavukcuoglu, K., Farabet, C.: Torch7: A matlab-like environment for machine learning. In: BigLearn, NIPS Workshop. (2011)

[34] Ioffe, S., Szegedy, C.: Batch Normalization: Accelerating Deep Network Training by Reducing Internal Covariate Shift. (2015)

Training Quantized Nets: A Deeper Understanding
Appendices

Here we present proofs of the lemmas and theorems presented in the main paper, as well as some additional experimental details and results.

A   Proof of Lemma 1

Proof. We want to bound the quantization error r^t. Consider the i-th entry in r^t denoted by r_i^t. Similarly, we define w_i^t and $\nabla \tilde{f}(w^t)_i$. Choose some random number $p \in [0,1]$. The stochastic rounding operation produces a value of r^t given by

$$
\begin{aligned}
r_i^t &= Q_s(w_i^t - \alpha_t \nabla \tilde{f}(w^t)_i) - w_i^t + \alpha_t \nabla \tilde{f}(w^t)_i \\
&= \Delta \cdot \begin{cases} \dfrac{\alpha_t \nabla \tilde{f}(w^t)_i}{\Delta} + \left\lfloor \dfrac{-\alpha_t \nabla \tilde{f}(w^t)_i}{\Delta} \right\rfloor + 1, & \text{for } p \le -\dfrac{\alpha_t \nabla \tilde{f}(w^t)_i}{\Delta} - \left\lfloor \dfrac{-\alpha_t \nabla \tilde{f}(w^t)_i}{\Delta} \right\rfloor, \\[3mm] \dfrac{\alpha_t \nabla \tilde{f}(w^t)_i}{\Delta} + \left\lfloor \dfrac{-\alpha_t \nabla \tilde{f}(w^t)_i}{\Delta} \right\rfloor, & \text{otherwise}, \end{cases} \\[3mm]
&= \Delta \cdot \begin{cases} -q + 1, & \text{for } p \le q, \\ -q, & \text{otherwise}, \end{cases}
\end{aligned}
$$

where we write $q = -\dfrac{\alpha_t \nabla \tilde{f}(w^t)_i}{\Delta} - \left\lfloor \dfrac{-\alpha_t \nabla \tilde{f}(w^t)_i}{\Delta} \right\rfloor$ and $q \in [0,1]$.

Now we have

$$
\begin{aligned}
\mathbb{E}_p\left[(r_i^t)^2\right] &\le \Delta^2((-q+1)^2 q + (-q)^2(1-q)) \\
&= \Delta^2 q(1-q) \\
&\le \Delta^2 \min\{q, 1-q\}.
\end{aligned}
$$

Because $\min\{q, 1-q\} \le \left| \dfrac{\alpha_t \nabla \tilde{f}(w^t)_i}{\Delta} \right|$, it follows that $\mathbb{E}_p\left[(r_i^t)^2\right] \le \Delta^2 \left| \dfrac{\alpha_t \nabla \tilde{f}(w^t)_i}{\Delta} \right| \le \Delta \left| \alpha_t \nabla \tilde{f}(w^t)_i \right|$.

Summing over the index i yields

$$
\begin{aligned}
\mathbb{E}_p\left\| r^t \right\|_2^2 &\le \Delta \alpha_t \left\| \nabla \tilde{f}(w^t) \right\|_1 \\
&\le \sqrt{d} \alpha_t \Delta \left\| \nabla \tilde{f}(w^t) \right\|_2. \tag{11}
\end{aligned}
$$

Now, $\left(\mathbb{E} \left\| \nabla \tilde{f}(w^t) \right\|_2 \right)^2 \le \mathbb{E} \left\| \nabla \tilde{f}(w^t) \right\|_2^2 \le G^2$. Plugging this into (11) yields

$$
\mathbb{E} \left\| r^t \right\|_2^2 \le \sqrt{d} \Delta \alpha_t G. \tag{12}
$$

$\square$

B   Proof of Theorem 1

Proof. From the update rule (6), we get:

$$
\begin{aligned}
w^{t+1} &= Q\left(w^t - \alpha_t \nabla \tilde{f}(w^t) \right) \\
&= w^t - \alpha_t \nabla \tilde{f}(w^t) + r^t,
\end{aligned}
$$

where r^t denotes the quantization used on the t-th iteration. Subtracting by the optimal $w^\star$, taking norm, and taking expectation conditioned on w^t, we get:

$$
\begin{aligned}
\mathbb{E}\|w^{t+1} - w^\star\|^2 &= \|w^t - w^\star\|^2 - 2\mathbb{E}\langle w^t - w^\star, \alpha_t \nabla \tilde{f}(w^t) - r^t \rangle + \mathbb{E}\|\alpha_t \nabla \tilde{f}(w^t) - r^t\|^2 \\
&= \|w^t - w^\star\|^2 - 2\alpha_t \langle w^t - w^\star, \nabla F(w^t) \rangle + \alpha_t^2 \mathbb{E}\|\nabla \tilde{f}(w^t)\|^2 + \mathbb{E}\|r^t\|^2 \\
&\le \|w^t - w^\star\|^2 - 2\alpha_t \langle w^t - w^\star, \nabla F(w^t) \rangle + \alpha_t^2 G^2 + \sqrt{d} \Delta \alpha_t G,
\end{aligned}
$$

where we use the bounded variance assumption, $\mathbb{E}[r^t] = 0$, and Lemma 1. Using the assumption that F is μ-strongly convex, we can simplify this to:

$$
\mathbb{E}\|w^{t+1} - w^\star\|^2 \le (1 - \alpha_t \mu)\|w^t - w^\star\|^2 - 2\alpha_t(F(w^t) - F(w^\star)) + \alpha_t^2 G^2 + \sqrt{d} \Delta \alpha_t G.
$$

Re-arranging the terms, and taking expectation we get:

$$2\alpha_t \mathbb{E}(F(w^t) - F(w^\star)) \leq (1 - \alpha_t\mu)\mathbb{E}\|w^t - w^\star\|^2 - \mathbb{E}\|w^{t+1} - w^\star\|^2 + \alpha_t^2 G^2 + \sqrt{d}\Delta\alpha_t G.$$

$$\Rightarrow \quad \mathbb{E}(F(w^t) - F(w^\star)) \leq \left(\frac{1}{2\alpha_t} - \frac{\mu}{2}\right)\mathbb{E}\|w^t - w^\star\|^2 - \frac{1}{2\alpha_t}\mathbb{E}\|w^{t+1} - w^\star\|^2 + \frac{\alpha_t}{2}G^2 + \frac{\sqrt{d}\Delta G}{2}.$$

Assume that the stepsize decreases with the rate $\alpha_t = 1/\mu(t+1)$. Then we have:

$$\mathbb{E}(F(w^t) - F(w^\star)) \leq \frac{\mu t}{2}\mathbb{E}\|w^t - w^\star\|^2 - \frac{\mu(t+1)}{2}\mathbb{E}\|w^{t+1} - w^\star\|^2 + \frac{1}{2\mu(t+1)}G^2 + \frac{\sqrt{d}\Delta G}{2}.$$

Averaging over $t = 0$ to T, we get a telescoping sum on the right hand side, which yields:

$$\frac{1}{T}\sum_{t=0}^{T}\mathbb{E}(F(w^t) - F(w^\star)) \leq \frac{G^2}{2\mu T}\sum_{t=0}^{T}\frac{1}{t+1} + \frac{\sqrt{d}\Delta G}{2} - \frac{\mu(T+1)}{2}\mathbb{E}\|w^{T+1} - w^\star\|^2$$

$$\leq \frac{(1 + \log(T+1))G^2}{2\mu T} + \frac{\sqrt{d}\Delta G}{2}.$$

Using Jensen's inequality, we have:

$$\mathbb{E}(F(\bar{w}^T) - F(w^\star)) \leq \frac{1}{T}\sum_{t=0}^{T}\mathbb{E}(F(w^t) - F(w^\star)),$$

where $\bar{w}^T = \frac{1}{T}\sum_{t=0}^{T} w^t$, the average of the iterates.

Thus the final convergence theorem is given by:

$$\mathbb{E}[F(\bar{w}^T) - F(w^\star)] \leq \frac{(1 + \log(T+1))G^2}{2\mu T} + \frac{\sqrt{d}\Delta G}{2}.$$

$\square$

C Proof of Theorem 2

Proof. From the update rule (6), we have,

$$w^{t+1} = Q(w^t - \alpha_t \nabla \tilde{f}(w^t)) = w^t - \alpha_t \nabla \tilde{f}(w^t) + r^t,$$

where r^t denotes the quantization error on the t-th iteration. Hence we have

$$\|w^{t+1} - w^\star\|^2 = \|w^t - \alpha_t \nabla \tilde{f}(w^t) + r^t - w^\star\|^2$$

$$= \|w^t - w^\star\|^2 - 2\langle w^t - w^\star, \alpha_t \nabla \tilde{f}(w^t) - r^t\rangle + \|\alpha_t \nabla \tilde{f}(w^t) - r^t\|^2.$$

Taking expectation, and using $\mathbb{E}[\tilde{f}(w^t)] = \nabla F(w^t)$ and $\mathbb{E}[r^t] = 0$, we have

$$\mathbb{E}\|w^{t+1} - w^\star\|^2 = \mathbb{E}\|w^t - w^\star\|^2 - 2\alpha_t\mathbb{E}\langle w^t - w^\star, \nabla F(w^t)\rangle + \mathbb{E}\|\alpha_t \nabla \tilde{f}(w^t) - r^t\|^2$$

$$= \mathbb{E}\|w^t - w^\star\|^2 - 2\alpha_t\mathbb{E}\langle w^t - w^\star, \nabla F(w^t)\rangle + \alpha_t^2\mathbb{E}\|\nabla \tilde{f}(w^t)\|^2 + \mathbb{E}\|r^t\|^2.$$

Using the bounded variance assumption $\mathbb{E}\|\nabla \tilde{f}(w^t)\|^2 \leq G^2$ and bounded quantization error in Lemma 1, we have

$$\mathbb{E}\|w^{t+1} - w^\star\|^2 \leq \mathbb{E}\|w^t - w^\star\|^2 - 2\alpha_t\mathbb{E}\langle w^t - w^\star, \nabla F(w^t)\rangle + \alpha_t^2 G^2 + \sqrt{d}\Delta\alpha_t G. \quad (13)$$

$F(x)$ is convex and hence $\langle \nabla F(x), x_t - x^\star\rangle \geq F(x_t) - F(x^*)$, which can be used in (13) to get

$$\mathbb{E}\|w^{t+1} - w^\star\|^2 \leq \mathbb{E}\|w^t - w^\star\|^2 - 2\alpha_t\mathbb{E}[F(w^t) - F(w^\star)] + \alpha_t^2 G^2 + \sqrt{d}\Delta\alpha_t G.$$

Re-arranging the terms, we have,

$$\mathbb{E}[F(w^t) - F(w^\star)] \leq \frac{1}{2\alpha_t}\left(\mathbb{E}\|w^t - w^\star\|^2 - \mathbb{E}\|w^{t+1} - w^\star\|^2\right) + \frac{\alpha_t}{2}G^2 + \frac{1}{2}\sqrt{d}\Delta G.$$

Accumulate from $t = 1$ to T to get

$$\sum_{t=1}^{T}\mathbb{E}[F(w^t) - F(w^\star)] \leq \frac{1}{2\alpha_1}\mathbb{E}\|w_1 - w^\star\|^2 + \sum_{t=1}^{T}\left(\frac{1}{2\alpha_t} - \frac{1}{2\alpha_{t-1}}\right)\mathbb{E}\|w^t - w^\star\|^2$$

$$+ \sum_{t=1}^{T}\frac{\alpha_t}{2}G^2 + \frac{T}{2}\sqrt{d}\Delta G.$$

Applying $\mathbb{E}\|w^t - w^\star\|^2 \leq D^2$ and $\sum_{t=1}^T \alpha_t \leq c\sqrt{T+1}$, we have

$$\sum_{t=1}^T \mathbb{E}[F(w^t) - F(w^\star)] \leq \frac{\sqrt{T}}{2c}D^2 + \frac{c\sqrt{T+1}}{2}G^2 + \frac{T}{2}\sqrt{d}\Delta G. \tag{14}$$

Since $F(w)$ is convex, we can set $\bar{w}^T = \frac{1}{T}\sum_{t=1}^T w^t$, and use Jensen's inequality to arrive at

$$\mathbb{E}[F(\bar{w}^T) - F(w^\star)] \leq \frac{1}{T}\sum_{t=1}^T \mathbb{E}[F(w^t) - F(w^\star)]. \tag{15}$$

Combine (14) and (15) to achieve

$$\mathbb{E}[F(\bar{w}^T) - F(w^\star)] \leq \frac{1}{2c\sqrt{T}}D^2 + \frac{\sqrt{T+1}}{2T}cG^2 + \frac{\sqrt{d}\Delta G}{2}.$$

$\square$

D   Proof of Theorem 3

Proof. From the update rule (7), we have,

$$w^{t+1} = w^t - \alpha_t \nabla \tilde{f}(Q(w^t)) = w^t - \alpha_t \nabla \tilde{f}(w^t + r^t).$$

Taking expectation conditioned on w^t and r^t, we have

$\mathbb{E}\|w^{t+1} - w^\star\|^2$
$= \mathbb{E}\|w^t - \alpha_t \nabla \tilde{f}(w^t + r^t) - w^\star\|^2$
$= \mathbb{E}\|w^t - \alpha_t \nabla \tilde{f}(w^t) + \alpha_t \nabla \tilde{f}(w^t) - \alpha_t \nabla \tilde{f}(w^t + r^t) - w^\star\|^2$
$= \|w^t - w^\star\|^2 - 2\alpha_t \mathbb{E}\langle w^t - w^\star, \nabla \tilde{f}(w^t)\rangle + 2\alpha_t \mathbb{E}\langle w^t - w^\star, \nabla \tilde{f}(w^t) - \nabla \tilde{f}(w^t + r^t)\rangle + \mathbb{E}\|\alpha_t \nabla \tilde{f}(w^t + r^t)\|^2$
$= \|w^t - w^\star\|^2 - 2\alpha_t \langle w^t - w^\star, \nabla F(w^t)\rangle + 2\alpha_t \langle w^t - w^\star, \nabla F(w^t) - \nabla F(w^t + r^t)\rangle + \alpha_t^2 \mathbb{E}\|\nabla \tilde{f}(w^t + r^t)\|^2$
$\leq \|w^t - w^\star\|^2 - 2\alpha_t \langle w^t - w^\star, \nabla F(w^t)\rangle + 2\alpha_t \|w^t - w^\star\|\|\nabla F(w^t) - \nabla F(w^t + r^t)\| + \alpha_t^2 G^2$
$\leq \|w^t - w^\star\|^2 - 2\alpha_t \langle w^t - w^\star, \nabla F(w^t)\rangle + 2\alpha_t L\|r^t\|\|w^t - w^\star\| + \alpha_t^2 G^2.$

Using $\|r^t\| \leq \sqrt{d}\Delta$ and the bounded domain assumption, we get

$$\mathbb{E}\|w^{t+1} - w^\star\|^2 \leq \|w^t - w^\star\|^2 - 2\alpha_t \langle w^t - w^\star, \nabla F(w^t)\rangle + 2\alpha_t L\sqrt{d}\Delta\|w^t - w^\star\| + \alpha_t^2 G^2$$
$$\leq \|w^t - w^\star\|^2 - 2\alpha_t \langle w^t - w^\star, \nabla F(w^t)\rangle + 2\alpha_t L\sqrt{d}\Delta D + \alpha_t^2 G^2.$$

Taking expectation, and following the same steps as in Theorem 2, we get the convergence result:

$$\mathbb{E}[F(\bar{w}^T) - F(w^\star)] \leq \frac{1}{2c\sqrt{T}}D^2 + \frac{\sqrt{T+1}}{2T}cG^2 + \sqrt{d}\Delta L D.$$

$\square$

E   Proof of Theorem 4

Proof. From the update rule (7), we get

$$w^{t+1} = w^t - \alpha_t \nabla \tilde{f}(Q(w^t))$$
$$= w^t - \alpha_t \nabla \tilde{f}(w^t + r^t)$$
$$= w^t - \alpha_t[\nabla \tilde{f}(w^t) + \nabla^2 \tilde{f}(w^t)r^t + \hat{r}^t]$$

where $\|\hat{r}^t\| \leq \frac{L_2}{2}\|r^t\|^2$ from our assumption on the Hessian. Note that in general r^t has mean zero while $\hat{r}^t$ does not. Using the same steps as in the Theorem 1, we get

$$\mathbb{E}\|w^{t+1} - w^\star\|^2 = \|w^t - w^\star\|^2 - 2\alpha_t \mathbb{E}\langle w^t - w^\star, \nabla \tilde{f}(w^t + r^t)\rangle + \alpha_t^2 \mathbb{E}\|\nabla \tilde{f}(w^t + r^t)\|^2.$$
$$\leq \|w^t - w^\star\|^2 - 2\alpha_t \mathbb{E}\langle w^t - w^\star, \nabla F(w^t) + \hat{r}^t\rangle + \alpha_t^2 G^2$$
$$= \|w^t - w^\star\|^2 - 2\alpha_t \mathbb{E}\langle w^t - w^\star, \nabla F(w^t)\rangle + \alpha_t^2 G^2 - 2\alpha_t \mathbb{E}\langle w^t - w^\star, \hat{r}^t\rangle$$

14

Assuming the domain has finite diameter D, and observing that the quantization error for BC-SGD can always be upper-bounded as $\|r^t\| \le \sqrt{d}\Delta$, we get:

$$-2\alpha_t \mathbb{E}\langle w^t - w^\star, \hat{r}^t \rangle \le 2\alpha_t D\mathbb{E}\|\hat{r}^t\| \le 2\alpha_t D\frac{L_2}{2}\|r^t\| \le \alpha_t DL_2\sqrt{d}\Delta.$$

Following the same steps as in Theorem 1, we get

$$\mathbb{E}[F(\bar{w}^T) - F(w^\star)] \le \frac{(1 + \log(T+1))G^2}{2\mu T} + \frac{DL_2\sqrt{d}\Delta}{2}.$$

$\square$

F Proof of Theorem 5

Proof. Let the matrix U_α be a partial transition matrix defined by $U_\alpha(x, x) = 0$, and $U_\alpha(x, y) = T_\alpha(x, y)$ for $x \ne y$. From U_α, we can get back the full transition matrix T_α using the formula

$$T_\alpha = I - \text{diag}(\mathbf{1}^T U_\alpha) + U_\alpha.$$

Note that this formula is essentially "filling in" the diagonal entries of T_α so that every column sums to 1, thus making T_α a valid stochastic matrix.

Let's bound the entries in U_α. Suppose that we begin an iteration of the stochastic rounding algorithm at some point x. Consider an adjacent point y that differs from x at only 1 coordinate, k, with $y_k = x_k + \Delta$. Then we have

$$
\begin{aligned}
U_\alpha(x, y) &= \frac{1}{\alpha}\int_0^\Delta p_{x,k}(x/\alpha)\frac{x}{\Delta}\,dx + \frac{1}{\alpha}\int_\Delta^{2\Delta} p_{x,k}(x/\alpha)\frac{2\Delta - x}{\Delta}\,dx \\
&= \frac{1}{\alpha}\int_0^{\Delta/\alpha} p_{x,k}(z)\frac{\alpha z}{\Delta}\alpha\,dz + \frac{1}{\alpha}\int_{\Delta/\alpha}^{2\Delta/\alpha} p_{x,k}(z)\frac{2\Delta - \alpha z}{\Delta}\alpha\,dz \\
&\le \alpha\int_0^{\Delta/\alpha} p_{x,k}(z)\frac{z}{\Delta}\,dz + \int_{\Delta/\alpha}^\infty p_{x,k}(z)\,dz \\
&= \alpha\int_0^\infty p_{x,k}(z)\frac{z}{\Delta}\,dz + O(\alpha^2).
\end{aligned}
\tag{16}
$$

Note we have used the decay assumption:

$$\int_\nu^\infty p_{x,k}(z) \le \frac{C}{\nu^2}.$$

Likewise, if $y_k = x_k - \Delta$, then the transition probability is

$$U_\alpha(x, y) = \alpha\int_{-\infty}^0 p_{x,k}(z)\frac{z}{\Delta}\,dz + O(\alpha^2),\tag{17}$$

and if $y_k = x_k \pm m\Delta$ for an integer $m > 1$,

$$U_\alpha(x, y) = O(\alpha^2).\tag{18}$$

We can approximate the behavior of U_α using the matrix

$$\tilde{U}(x, y) = \begin{cases} \int_0^\infty p_{x,k}(z)\frac{z}{\Delta}\,dz, \text{if } x \text{ and } y \text{ differ only at coordinate } k, \text{ and } y_k = x_k + \Delta \\ \int_{-\infty}^0 p_{x,k}(z)\frac{z}{\Delta}\,dz, \text{if } x \text{ and } y \text{ differ only at coordinate } k, \text{ and } y_k = x_k - \Delta \\ 0, \text{otherwise.} \end{cases}$$

Define the associated markov chain transition matrix

$$\tilde{T}_{\alpha_0} = I - \alpha_0 \cdot \text{diag}(\mathbf{1}^T \tilde{U}) + \alpha_0\tilde{U},\tag{19}$$

where α_0 is the largest scalar such that the stochastic linear operator $\tilde{T}_{\alpha_0}$ has non-negative entries. For $\alpha < \alpha_0$, $\tilde{T}_\alpha$ has non-negative entries and column sums equal to 1; it thus defines the transition operator of a markov chain. Let $\tilde{\pi}$ denote the stationary distribution of the markov chain with transition matrix $\tilde{T}_{\alpha_0}$.

We now claim that $\tilde{\pi}$ is also the stationary distribution of $\tilde{T}_\alpha$ for all $\alpha < \alpha_0$. We verify this by noting that

$$
\begin{aligned}
\tilde{T}_\alpha &= (I - \alpha \cdot \text{diag}(\mathbf{1}^T \tilde{U})) + \alpha\tilde{U} \\
&= (1 - \frac{\alpha}{\alpha_0})I + \frac{\alpha}{\alpha_0}[I - \alpha_0 \cdot \text{diag}(\mathbf{1}^T \tilde{U}) + \alpha_0\tilde{U}] \\
&= (1 - \frac{\alpha}{\alpha_0})I + \frac{\alpha}{\alpha_0}\tilde{T}_{\alpha_0},
\end{aligned}
\tag{20}
$$

15

and so $\tilde{T}_\alpha \tilde{\pi} = (1 - \frac{\alpha}{\alpha_0})\tilde{\pi} + \frac{\alpha}{\alpha_0}\tilde{\pi} = \tilde{\pi}$.

Recall that T_α is the transition matrix for the Markov chain generated by the stochastic rounding algorithm with learning rate α. We wish to show that this markov chain is well approximated by $\tilde{T}_\alpha$. Note that

$$T_\alpha(x, y) = \prod_{k, x_k \neq y_k} T_\alpha(x, x + (y_k - x_k)\Delta e_k) \leq O(\alpha^2)$$

when x, y differ at more than 1 coordinate. In other words, transitions between multiple coordinates simultaneously become vanishingly unlikely for small α. When x and y differ by exactly 1 coordinate, we know from (16) that

$$T_\alpha(x, y) = \alpha U(x, y) + O(\alpha^2).$$

These observations show that the off-diagonal elements of T_α are well approximated (up to uniform $O(\alpha^2)$ error) by the corresponding elements in αU. Since the columns of T_α sum to one, the diagonal elements are well approximated as well, and we have

$$T_\alpha = (I - \alpha \cdot \operatorname{diag}(\mathbf{1}^T U)) + \alpha U + O(\alpha^2) = \tilde{T}_\alpha + O(\alpha^2).$$

To be precise, the notation above means that

$$|T_\alpha(x, y) - \tilde{T}_\alpha(x, y)| < C\alpha^2, \tag{21}$$

for some C that is uniform over (x, y).

We are now ready to show that the stationary distribution of T_α exists and approaches $\tilde{\pi}$. Re-arranging (20) gives us

$$\alpha_0 \tilde{T}_\alpha + (\alpha - \alpha_0)I = \alpha \tilde{T}_{\alpha_0}.$$

Combining this with (21), we get

$$\left\| \alpha_0 T_\alpha + (\alpha - \alpha_0)I - \alpha \tilde{T}_{\alpha_0} \right\|_\infty < O(\alpha^2),$$

and so

$$\left\| \frac{\alpha_0}{\alpha} T_\alpha + (1 - \frac{\alpha_0}{\alpha})I - \tilde{T}_{\alpha_0} \right\|_\infty < O(\alpha). \tag{22}$$

From (22), we see that the matrix $\frac{\alpha_0}{\alpha} T_\alpha + (1 - \frac{\alpha_0}{\alpha})I$ approaches $\tilde{T}_{\alpha_0}$. Note that $\tilde{\pi}$ is the Perron-Frobenius eigenvalue of $\tilde{T}_{\alpha_0}$, and thus has multiplicity 1. Multiplicity 1 eigenvalues/vectors of a matrix vary continuously with small perturbations to that matrix (Theorem 8, p130 of [30]). It follows that, for small α, $\frac{\alpha_0}{\alpha} T_\alpha + (1 - \frac{\alpha_0}{\alpha})I$ has a stationary distribution, and this distribution approaches $\tilde{\pi}$. The leading eigenvector of $\frac{\alpha_0}{\alpha} T_\alpha + (1 - \frac{\alpha_0}{\alpha})I$ is the same as the leading eigenvector of T_α, and it follows that T_α has a stationary distribution that approaches $\tilde{\pi}$.

Finally, note that we have assumed $\int_0^{C_2} p_{x,k}(z)\, dz > 0$ and $\int_{-C_2}^0 p_{x,k}(z)\, dz > 0$. Under this assumption, for $\alpha < \frac{1}{C_2}$, $\tilde{T}_{\alpha_0}(x, y) > 0$ whenever x, y are neighbors the differ at a single coordinate. It follows that every state in the Markov chain $\tilde{T}_{\alpha_0}$ is accessible from every other state by traversing a path of non-zero transition probabilities, and so $\tilde{\pi}(x) > 0$ for every state x.

$\square$

G   Proof of Theorem 6

Proof. Given some distribution π over the states of the markov chain, and some set A of states, let $[\pi]_A = \sum_{a \in A} \pi(a)$ denote the measure of A with respect to π.

Suppose for contradiction that the mixing time of the chain remains bounded as α vanishes. Then we can find an integer M_ϵ that upper bounds the ϵ-mixing time for all α. By the assumption of the theorem, we can select some set of states A with $[\tilde{\pi}]_A > \epsilon$, and some starting state $y \notin A$. Let e be a distribution (a vector in the finite-state case) with $e_y = 1$, $e_k = 0$ for $k \neq y$. Note that $[e]_A = 0$ because $y \notin A$. Then

$$\left| [e]_A - [\tilde{\pi}]_A \right| > \epsilon.$$

Note that, as $\alpha \to 0$, we have $\|T_\alpha - \tilde{T}_\alpha\| \to 0$ and thus $\|T_\alpha^{M_\epsilon} - \tilde{T}_\alpha^{M_\epsilon}\| \to 0$. We also see from the definition of $\tilde{T}_\alpha$ in (19), $\lim_{\alpha \to 0} \tilde{T}_\alpha = I$. It follows that

$$\lim_{\alpha \to 0} \left| [T_\alpha^{M_\epsilon} e]_A - [\tilde{\pi}]_A \right| = \left| [e]_A - [\tilde{\pi}]_A \right| > \epsilon,$$

and so for some α the inequality (10) is violated. This is a contradiction because it was assumed M_ϵ is an upper bound on the mixing time.

$\square$

H Additional Experimental Details & Results

H.1 Neural Net Architecture & Training Details

We train image classifiers using two types of networks, VGG-like CNNs [24] and Residual networks [25], on CIFAR-10/100 [31] and ImageNet 2012 [26]. VGG-9 on CIFAR-10 consists of 7 convolutional layers and 2 fully connected layers. The convolutional layers contain 64, 64, 128, 128, 256, 256 and 256 of 3×3 filters respectively. There is a Batch Normalization and ReLU after each convolutional layer and the first fully connected layer. The details of the architecture are presented in Table 2. VGG-BC is a high-capacity network used for the original BC method [5], which contains 6 convolutional layers and 3 linear layers. We use the same architecture as in [5] except using softmax and cross-entropy loss instead of SVM and squared hinge loss, respectively. The details of the architecture are presented in Table 3. ResNets-56 has 55 convolutional layers and one linear layer, and contains three stages of residual blocks where each stage has the same number of residual blocks. We also create a wide ResNet-56 (WRN-56-2) that doubles the number of filters in each residual block as in [32]. ResNets-18 for ImageNet has the same description as in [25].

The default minibatch size is 128. However, the big-batch SR-ADAM method adopts a large minibatch size (512 for WRN-56-2 and ResNet-18 and 1024 for other models). Following [5], we do not use weight decay during training. We implement all models in Torch7 [33] and train the quantized models with NVIDIA GPUs.

Similar to [3], we only quantize the weights in the convolutional layers, but not linear layers, during training. Binarizing linear layers causes some performance drop without much computational speedup. This is because fully connected layers have very little computation overhead compared to Conv layers. Also, for state-of-the-art CNNs, the number of FC parameters is quite small. The number of params of Conv/FC layers for CNNs in Table 1 are (in millions): VGG-9: 1.7/1.1, VGG-BC: 4.6/9.4, ResNet-56: 0.84/0.0006, WRN-56-2: 3.4/0.001, ResNet-18: 11.2/0.5. While the VGG-like nets have many FC parameters, the more efficient and higher performing ResNets are almost entirely convolutional.

Table 2: VGG-9 on CIFAR-10.

layer type	kernel size	input size	output size
Conv_1	3×3	$3 \ \times 32 \times 32$	$64 \ \times 32 \times 32$
Conv_2	3×3	$64 \ \times 32 \times 32$	$64 \ \times 32 \times 32$
Max Pooling	2×2	$64 \ \times 32 \times 32$	$64 \ \times 16 \times 16$
Conv_3	3×3	$64 \ \times 16 \times 16$	$128 \times 16 \times 16$
Conv_4	3×3	$128 \times 16 \times 16$	$128 \times 16 \times 16$
Max Pooling	2×2	$128 \times 16 \times 16$	$128 \times 8 \ \times 8$
Conv_5	3×3	$128 \times 8 \ \times 8$	$256 \times 8 \ \times 8$
Conv_6	3×3	$256 \times 8 \ \times 8$	$256 \times 8 \ \times 8$
Conv_7	3×3	$256 \times 8 \ \times 8$	$256 \times 8 \ \times 8$
Max Pooling	2×2	$256 \times 8 \ \times 8$	$256 \times 4 \ \times 4$
Linear	1×1	1×4096	1×256
Linear	1×1	1×256	1×10

Table 3: VGG-BC for CIFAR-10.

layer type	kernel size	input size	output size
Conv_1	3×3	$3 \ \times 32 \times 32$	$128 \times 32 \times 32$
Conv_2	3×3	$128 \times 32 \times 32$	$128 \times 32 \times 32$
Max Pooling	2×2	$128 \times 32 \times 32$	$128 \times 16 \times 16$
Conv_3	3×3	$128 \times 16 \times 16$	$256 \times 16 \times 16$
Conv_4	3×3	$256 \times 16 \times 16$	$256 \times 16 \times 16$
Max Pooling	2×2	$256 \times 16 \times 16$	$256 \times 8 \ \times 8$
Conv_5	3×3	$256 \times 8 \ \times 8$	$512 \times 8 \ \times 8$
Conv_6	3×3	$512 \times 8 \ \times 8$	$512 \times 8 \ \times 8$
Max Pooling	2×2	$512 \times 8 \ \times 8$	$512 \times 4 \ \times 4$
Linear	1×1	1×8192	1×1024
Linear	1×1	1×1024	1×1024
Linear	1×1	1×1024	1×10

H.2 Convergence Curves

The convergence curves for training and testing errors reported in Table 1 are shown in Figure 6.
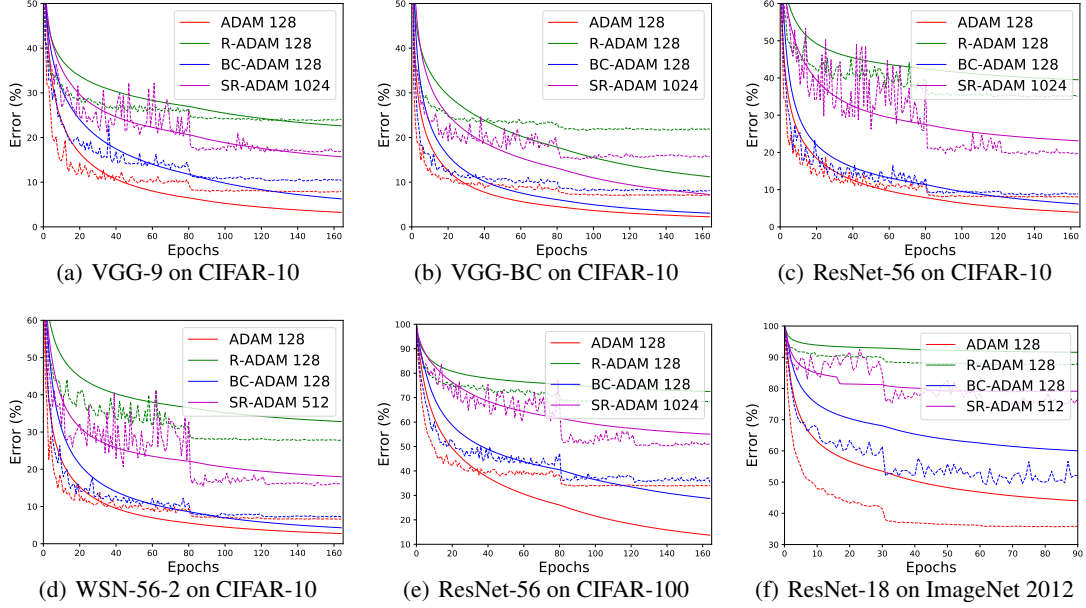
Figure 6: Training and testing errors of different training methods for VGG-9, VGG-BC, ResNet-56, Wide-ResNet-56-2 and ResNet-18. The solid line is the training error and the dashed line is the testing error.

H.3 Weight Initialization and Learning Rate

For experiments on SR-Adam and R-Adam, the weights of convolutional layers are intitialized with random Rademacher (± 1) variables. The authors of BC [5] adopt a small initial learning rate (0.003) and it takes 500 epochs to converge. It is observed that large binary weights ($\Delta = 1$) will generate small gradients when batch normalization is used [34], hence a large learning rate is necessary for faster convergence. We experiment with a larger learning rate (0.01) and find it converges to the same performance within 160 epochs, comparing with 500 epochs in the original paper [5].

H.4 Weight Decay

Figure 7 shows the effect of applying weight decay to BC-ADAM. As shown in Figure 7(a), BC-ADAM with 1e-5 weight decay yields worse performance compared to zero weight decay. Applying weight decay in BC-ADAM will shrink w_r to 0, as well as increase the distance between w_b and w_r. Figure 7(b) and 7(c) shows the distance between w_b and w_r during training. With 1e-5 weight decay, the average weight difference between w_b and w_r approaches 1, which indicates w_r is close to zero. Weight decay cannot "decay" the weight of SR as $\|w_b\|_2$ is the same for all binarized networks.
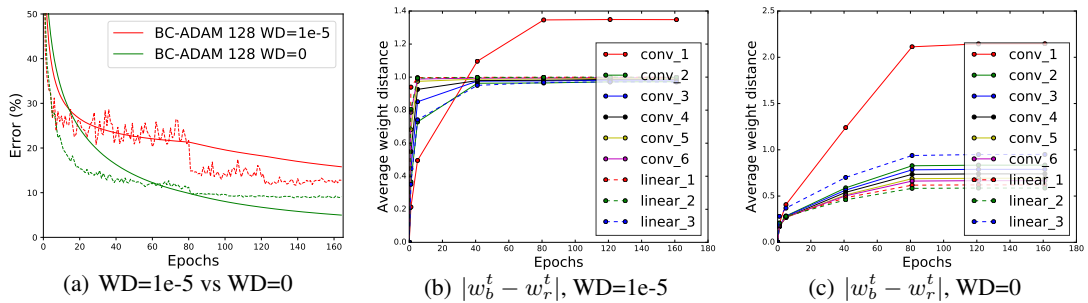

Figure 7: The effect of weight decay (WD) on BC-ADAM for training VGG-BC. The y-axis of (b) and (c) is the averaged weight difference between the binary weights w_b and the real-valued weights w_r, i.e., $\frac{1}{d}\|w_b^t - w_r^t\|_1$. where d is the number of weights in w_b.